

**STUDY OF STRESS WAVE PROPAGATION PATH AND DEPTH  
IDENTIFICATION IN CRACKED WOOD BASED ON ACOUSTIC EMISSION  
AND COMSOLSIMULATION**

CHUMIN CHEN<sup>1,2</sup>, MING LI<sup>3</sup>, SAIYIN FANG<sup>2,1</sup>, JIALONG ZHAO<sup>1</sup>, XIN ZHANG<sup>1</sup>,  
FANGYONG LU<sup>1</sup>, TINGTING DENG<sup>1</sup>, BO ZHANG<sup>4</sup>

<sup>1</sup>SOUTHWEST FORESTRY UNIVERSITY, YUNNAN

<sup>2</sup>YUNNAN KEY LABORATORY OF WOOD ADHESIVE AND GLUED PRODUCTS

<sup>3</sup>ANHUI POLYTECHNIC UNIVERSITY, ANHUI

<sup>4</sup>DALIAN UNIVERSITY OF TECHNOLOGY

CHINA

(RECEIVED JULY 2024)

## **ABSTRACT**

The propagation velocity models were built using AE sensors to capture stress wave on pine specimen surface. On the different specimens, cracks were made in different numbers and the depth was gradually increased from 0 mm to 90 mm at 10 mm intervals. AE experiment was combined with COMSOL to investigate propagation path. The results show that R-squared is 0.996 when fitting tangent of angle to propagation velocity. At smaller crack depths, stress wave is diffracted around crack tip and then continues to propagate in to sensor along a straight line. However, as the crack depth increases, the reflected wave at the end face will arrive at the detection location faster with significantly weaker diffraction. The area with dimensions of 20×10 mm was identified about the crack tip by crack identification method.

**KEYWORDS:** Cracked wood, acoustic emission, finite element analysis, stress waves, propagation paths.

## **INTRODUCTION**

Defects in wood are an unavoidable engineering problem due to the fact that the stability of the structure is impacted by defective features such as cracks and scars in the wood. In the acoustic inspection field, defects and damages in wood cause noticeable effects on stress waves (Xu et al. 2023; Zhang et al. 2024). Acoustic emission (AE) is a phenomenon

that is characterized by the rapid release of energy from a local acoustic source when a material is fractured, resulting in a stress wave. Accordingly, the AE signal is a kind of stress wave, and it is reliable to assess the damage defects of wood by the AE signal. As a non-destructive testing (NDT) technology, AE technology can continuously monitor the signals of internal object in real time, which is widely used in the fields of rocks(Zhang et al. 2020), coal mines(Dai et al. 2023), concrete(Ren et al. 2023) and so on.

Currently, researchers have conducted a series of studies and explorations on the impact of cracks from the AE signals in wood components. However, most of them have focused on investigating the damage fracture mode and the fracture state(Wang et al. 2020; Gao et al. 2022). While few have investigated the propagation path of stress waves in cracked wood. In fact, exploring the propagation paths of stress waves and extracting the information carried by the AE signals to further analyze the damage fracture mechanism provide an effective reference for defect damage identification. On intact wood surfaces, it is dependable to regard the propagation path of a stress wave along a straight line as the shortest path(Sahu and Bhattacharyay 2018). However, the propagation path becomes more complicated when there are discontinuous interfaces (such as cracks, holes, and other defects) in the material. Therefore, it is more difficult to explore the propagation paths by AE experiment solely. With the emergence of numerical techniques and the improvement of computational power, the research method of using finite elements to model and simulate physical and chemical processes in different fields has been favored by scholars. In AE field, an effective method has been provided to explore the propagation paths of stress waves based on finite element simulation, which helps to observe the complex propagation process in wood(Han et al. 2020; Yang et al. 2023).

Pine wood was used as the research object in this study. The propagation path of the AE signal on the wood surface with cracks was explored based on the AE experiments and COMSOL software simulation by the method of stress wave detection. Moreover, the crack tip location in the wood is determined based on the time difference in different propagation paths. First, the AE source was simulated using the pencil-lead break (PLB) method according to ASTM-E976. The signals were collected using AE sensors. Further, the variations of time difference of stress waves in cracked specimens with different depths and numbers were examined. Secondly, the propagation process was simulated by COMSOL simulation software to explore the propagation path of stress waves. Subsequently, the location of the cracks was identified based on the time difference the stress waves under different paths.

## **MATERIAL AND METHODS**

### **AE experimental material and equipment**

In this study, pinesawn timber with air-dried and no surface defects was used as the experimental material with the density of 409.82 kg/m<sup>3</sup> and moisture content of 11.5%. Specimens with dimensions of 300×30×100 mm (L×W×H) were intercepted from the experimental material and recorded as T<sub>1</sub>, T<sub>2</sub>, respectively. Cracks of length 1 mm in the L x W

side of the specimens were produced by sawing with a saw blade, which was cut at an angle of  $90^\circ$  to the wood grain. The number of cracks on specimen  $T_1$  was 1, while the number on specimen  $T_2$  was 2. The depth of the cracks was increased gradually from 0 mm to 90 mm with the interval of 10 mm. The specific crack parameters of the specimens (Tab. 1).

Tab. 1: Cracking parameters of the specimens.

Specimens	Numbers	Intervals / (mm)	Widths ( $L_0$ ) / (mm)	Depths ( $H_0$ ) / (mm)
$T_1$	1	—	1	0, 10, 20, 30, 40, 50,
$T_2$	2	40		60, 70, 80, 90

A multi-channel AE signal acquisition system was built using NI USB-6366 high-speed acquisition card and LabVIEW software. During the experiment, the voltage range of the output of the acquisition card was set to (-10 V, +10 V). For long-distance signal transmission, a PAI preamplifier with a gain of 40 dB was equipped and an RS-2A single-ended resonant transducer with a resonant frequency of 150 kHz was adopted. According to Shannon's sampling theorem, the sampling frequency  $f_s$  is at least two times higher than the highest frequency  $f_{\max}$  of the original signal in order to ensure that the analog signal is undistorted. The AE signals in the wood are mainly concentrated in 20 kHz-220 kHz (Li et al. 2021; Xu et al. 2023), so the sampling frequency was set to 2 MHz to improve the accuracy in the time-frequency domain.

### AE experimental methods

According to the study of Afoutou et al. (2023), the propagation velocity and angle of stress waves on the wood surface are highly connected as wood is an anisotropic material. The propagation velocity at different angles is the key to explore the propagation path of the stress wave. Therefore, the experimental program was divided into two parts. In the first part, the propagation velocity was modeled on the intact specimen surface (Fig. 1); in the second part, the propagation path was explored on the specimen with cracks (Fig. 2).

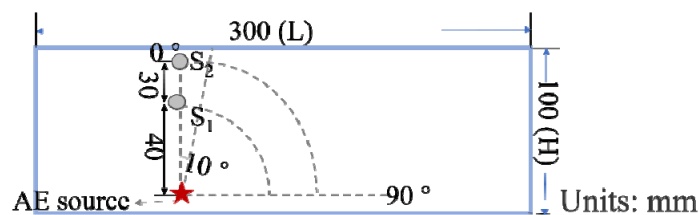


Fig. 1: Experimental diagram to model the propagation velocity.

In order to model the propagation velocity of the stress wave, the experimental diagram was designed as shown in Fig. 1. An analog AE source was generated on the surface of specimen  $T_1$  by the method of Pencil-lead break (PLB) and the signal was collected by the AE sensor. PLB tests were referenced to the ASTM-E976 standard in America. The lead core with diameter of 0.5 mm and elongation of 2.5 mm forms an  $30^\circ$  angle with the specimen surface. The AE source was considered as the circle center. Two concentric quarter circles with radii of 40 and 70 mm were set up. The sensors  $S_1$  and  $S_2$  were placed on the circumference of

the circles, co-linear with the AE source. For uniform presentation, the  $0^\circ$  line was set as shown in Fig. 1. The propagation direction of  $90^\circ$  was divided into 10 directions at  $10^\circ$  intervals. The propagation velocity of the stress wave at different angles was measured using the Time Difference of Arrival (TDOA) method (Wang et al. 2020).

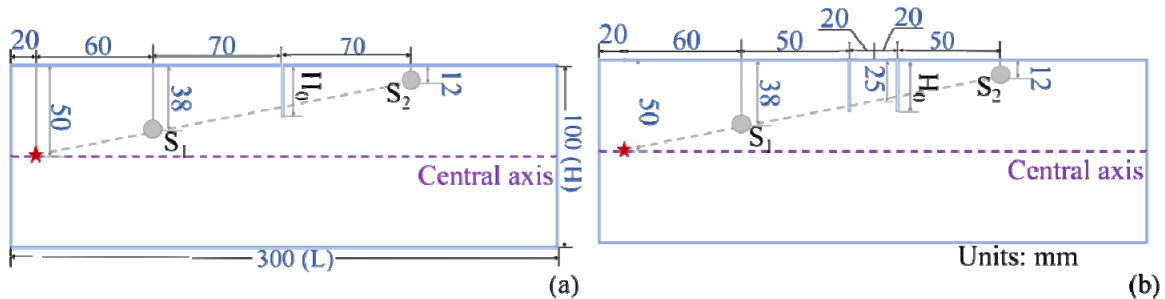


Fig. 2: Experimental diagram to investigate the propagation path of the stress wave, (a) specimen  $T_1$ , (b) specimen  $T_2$ . Units: mm.

In order to investigate the propagation path of the stress wave, the experimental diagram was designed as shown in Fig. 2. Firstly, the analog AE source was generated on the transverse median axis on the surfaces of specimens  $T_1$  and  $T_2$ , which was 20 mm away from the left end face. Next, with centering the AE source, the sensors  $S_1$ ,  $S_2$  were placed in the direction at an angle of  $11^\circ$  to the central axis. A regular crack of depth  $H_0$  existed between the sensors to analyze the propagation path of the stress wave as it passed through the crack. In every specimen, the sensor was co-linear with the AE source.

### COMSOL simulation modeling

In order to investigate the propagation path when stress waves propagate in wood, COMSOL simulation software was used to establish the numerical models of different numbers and depths cracks, respectively. The blue boundary (Fig. 3) was set as a low-reflection boundary in order to reduce the interference of the reflected echoes due to the fact that the propagation paths of longitudinal wave as it passes through the cracks were mainly investigated in the numerical simulation model. Moreover, the maximum cell size  $l_{\max}$  of the finite element mesh and the wavelength  $\lambda$  satisfied at least  $l_{\max} \leq \lambda/3$  (Zhang et al. 2015). For the accuracy of the simulation and the efficiency of the calculation,  $l = \lambda/20$  was set. The performance parameters in the L and H directions are different because of the anisotropic nature of wood, as shown in Tab. 2. The numerical model was established as shown in Fig. 3. For comparison with the AE experiment, the dimensions of the model were the same as the specimen dimensions in the 1.1 experimental program. In the model, a sinusoidal pulse signal modulated by the Hanning window was used as the excitation signal and its functional expression was:

$$F(t) = \begin{cases} \frac{1}{2} \left[ 1 - \cos\left(\frac{2\pi f_0}{N} t\right) \right] \times \left[ \sin\left(\frac{2\pi f_0}{N} t\right) \right], & t \in \left[ 0, \frac{N}{f_0} \right] \\ 0, & t \in \left( \frac{N}{f_0}, 2e^{-4} \right) \end{cases} \quad \#(1)$$

where:  $f_0$  is the frequency of the excitation function,  $f_0=200$  kHz;  $t$  is the time with unit as s; N is the number of cycles of the pulse signal,  $N=5$ .

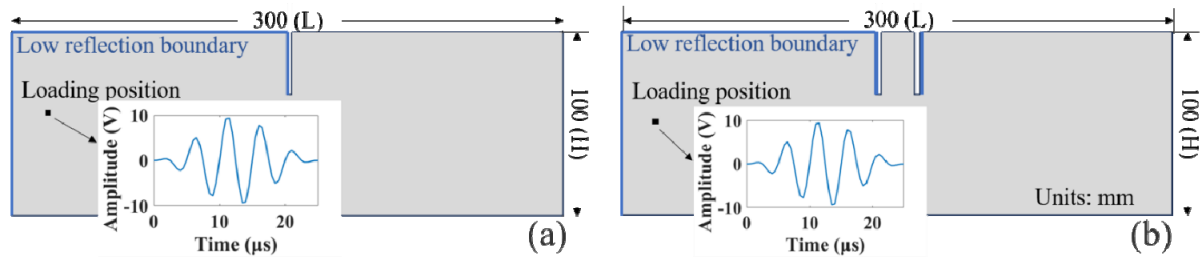


Fig. 3: Numerical simulation model, (a) specimen  $T_1$ , (b) specimen  $T_2$ .

Tab. 2: Parameters of material properties.

	Young's modulus (MPa)	Poisson ratio	Shear modulus (MPa)
L direction	$E_L=11583$	$\nu_L=0.47$	$G_L=690$
H direction	$E_R=896$	$\nu_R=0.43$	$G_R=758$

Note: Parameters are derived from the elastic constants of coniferous wood in Wood Science(Liu et al. 2012). Pine wood is coniferous.

## RESULTS AND DISCUSSION

### AE experiment results and analysis

#### The propagation velocity model of stress wave

According to Fig. 1, 10 PLB tests were conducted at each angle to calculate the propagation velocity of the stress wave using the TDOA method, and the average value of the velocity for the 10 PLB tests was obtained, as shown in Tab. 3. The trend curve of the propagation velocity ( $v$ ) with angle ( $\alpha$ ) of the stress wave was fitted using the least squares method, and the fitted curve was shown in Fig. 4 with the fitting equation:

$$v = \frac{1}{a + b e^{-c \tan(\alpha)}} \#(2)$$

where: a, b, c are constants,  $a = 0.1963$ ,  $b = 0.7014$ ,  $c = 0.8237$ . The premise assumption for the modeling of the study is that the propagation of the stress wave is linear(Afoutou et al. 2023).

Tab. 3: Stress wave propagation velocity at different angles

Angles (°)	0	10	20	30	40	50	60	70	80	90
Velocity (km/s)	1.16	1.28	1.33	1.46	1.80	2.28	2.62	3.75	4.91	4.97

Actually, the stress wave cannot propagate through the crack, but will be emitted and refracted at the interface generated by the crack and change the propagation direction(Li et al. 2019). Moreover, the propagation direction of the stress wave changes as a consequence of the change in the length of the tracheids near the defects when cracks are present in the wood. Hence, the propagation velocity of the stress wave in different directions is critical

when the time difference between the AE sensors is used to explore the propagation path of on the cracked wood. Besides, different modes waves such as longitudinal, transverse, and surface waves are generated when stress waves propagate on the wood surface. Among the multiple modes of waves, the propagation velocity of longitudinal waves is the fastest (Yu et al. 2023). Therefore, it is often used to detect defects in wood. The article establishes the propagation velocity model of longitudinal wave according to Eq. 4. From Fig. 4, the propagation velocity model is a saturation curve in which the velocity is constantly changing with increase in angle tangent, and the R-squared is 0.996. According to the fitted curve, the value of velocity increases rapidly when  $\tan(\alpha)$  is less than 3 approximately, and is slowly stabilized when  $\tan(\alpha)$  is greater than 3 approximately.

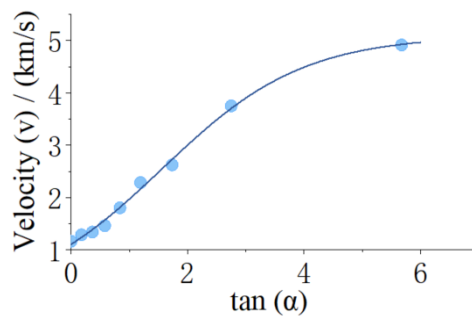


Fig. 4: Propagation velocity model of stress waves.

Wei et al. fitted the propagation velocity with angle of a stress wave in wood as a one-dimensional quadratic function with R-squared ranging from 0.83 to 0.97 (Wei et al. 2019; Wei et al. 2021). In this article, the R-squared is greater than 0.99 when fitting through Eq. 4, which will provide a meaningful basis for the following study of propagation paths.

#### *Effect on the propagation path of stress waves from cracks*

Based on the propagation velocity model of stress waves, the effect on the propagation path of stress waves by cracks was investigated. The propagation paths  $P_1$ ,  $P_2$ , and  $P_3$  of the stress waves were assumed based on the basic propagation behavior for diffraction and reflection, as shown in Fig. 5.  $P_1$  means that the stress wave propagates along straight line;  $P_2$  means that the diffracted wave generated at the crack tip is received by the AE sensor first;  $P_3$  means that the reflected wave at the end face is received first by the AE sensor from the diffraction at the crack. The study calculated the velocity under the assumed propagation path based on Eq. 2 and the time difference in combination with the propagation distance; while the actual propagation time difference on the surfaces of  $T_1$  and  $T_2$  during the PLB test was calculated by the Time Difference of Arrival (TDOA) method, which are shown in Tab. 4 and Tab. 5, respectively. The error in the time difference between the actual and assumed propagation paths is:

$$\varepsilon = \frac{t' - t}{t} \#(3)$$

where:  $t$  - the time difference in the actual path with units of  $\mu\text{s}$ ;  $t'$  - the time difference in

the assumed path with units of  $\mu\text{s}$ ;  $\varepsilon$ - the error of the two paths mentioned above.

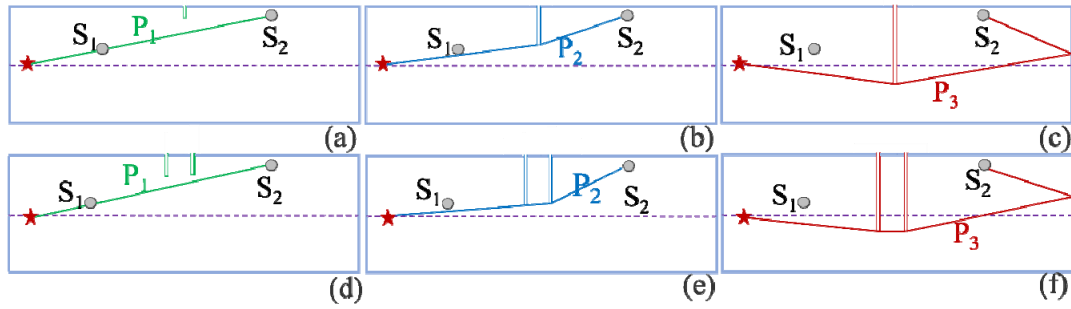


Fig. 5: Stress wave propagation path on the crack specimen surface.

From Tab.4 and Tab. 5, the propagation path of the stress wave is determined according to the principle of error minimization. In the case of  $H_0 \leq 20$  mm, the stress wave propagates along a straight line, in the path  $P_1$ . With the increase of crack depth, the diffraction phenomenon of the stress wave occurs at the crack while the diffracted wave is generated. In the case of  $20 \text{ mm} \leq H_0 \leq 40$  mm, the diffracted wave that continues to propagate along a straight line is detected by the AE sensor, in which case the stress wave propagates under the path  $P_2$ . Meanwhile, the reflected wave from the right end face is also detected by the AE sensor, which comes from the diffracted wave from the crack tip propagating along the grain direction. In the case of  $H_0 \geq 50$  mm, the reflected stress wave passing through the end face reaches the sensor faster than the diffracted wave propagating along the straight line due to the anisotropic characteristics of wood, in the path  $P_3$ . In addition, in the case of  $40 \text{ mm} \leq H_0 \leq 50$  mm, both  $P_2$  and  $P_3$  are reasonable paths.

In fact, pine wood belongs to coniferous wood, a layered structural material composed of axial tracheids (Atreya et al. 2023). On its surface, stress waves are more likely to propagate along the longitudinal direction of the surface of the wood. In the longitudinal direction, the propagation medium mainly includes axial tracheids, wood rays, parenchyma, etc., therefore the damping effect encountered by the stress wave is smaller and the propagation velocity is faster. Thus,  $P_2$  and  $P_3$  are the main propagation paths of the stress wave when the wood tracheids are cut off by the cracks. And The AE signal received by the sensor is significantly delayed. Similarly, Huang (2021), Wang (2020) and others showed that the time difference of the stress wave increases with the dimensions of the crack.

In addition, the time difference in the actual propagation path of the stress wave is greater than 90% of the assumed propagation path, based on the absolute error  $\varepsilon$ . The reason is that during the crack-making process, minor damage, such as extrusion and extension cause the change in the arrangement of the tracheid structure near the crack (Qin et al. 2024). Thus, the propagation mode and propagation medium of the stress wave change, which leads to a longer actual duration of the stress wave in the cracked specimen.

Tab. 4: Time difference between  $S_1$  and  $S_2$  on the surface of specimen  $T_1$ .

$H_0$ (mm)	0	10	20	30	40	50	60	70	80	90
Actual path ( $\mu\text{s}$ )	32.6	32.8	33.5	35.6	38.9	60.9	75.2	93.5	107.5	122.3

$P_1$ ( $\mu\text{s}$ )	32.3	32.3	32.3	32.3	32.3	32.3	32.3	32.3	32.3	32.3
$\varepsilon$ (%)	<b>0.9</b>	<b>1.5</b>	<b>3.6</b>	9.3	16.7	47.0	57.0	65.5	67.0	73.6
$P_2$ ( $\mu\text{s}$ )	59.4	51.5	47.7	33.0	35.8	40.9	48.2	57.2	68.3	79.9
$\varepsilon$ (%)	82.2	57.0	42.4	<b>7.4</b>	<b>7.9</b>	32.8	35.8	38.8	36.5	34.7
$P_3$ ( $\mu\text{s}$ )	89.0	82.7	81.5	61.1	58.8	62.8	68.4	75.3	89.5	94.6
$\varepsilon$ (%)	173	152	143	71.6	51.3	<b>3.1</b>	<b>9.0</b>	<b>19.5</b>	<b>16.8</b>	<b>22.6</b>

Tab. 5: Time difference between  $S_1$  and  $S_2$  on the surface of specimen  $T_2$ .

$H_0$ (mm)	0	10	20	30	40	50	60	70	80	90
Actual path ( $\mu\text{s}$ )	32.9	34.6	33.4	35.3	45.5	54.8	80.4	100.0	109.9	122.9
$P_1$ ( $\mu\text{s}$ )	32.3	32.3	32.3	32.3	32.3	32.3	32.3	32.3	32.3	32.3
$\varepsilon$ (%)	<b>1.8</b>	<b>6.8</b>	<b>3.2</b>	8.5	29.0	41.1	59.8	67.7	70.1	73.7
$P_2$ ( $\mu\text{s}$ )	58.6	56.2	52.7	33.9	37.6	43.8	50.8	60.9	72.4	84.3
$\varepsilon$ (%)	78.1	62.4	57.8	<b>1.3</b>	<b>7.9</b>	11.1	29.6	39.1	37.5	38.7
$P_3$ ( $\mu\text{s}$ )	87.5	81.5	68.0	58.2	62.0	63.7	68.3	76.8	89.5	101.8
$\varepsilon$ (%)	166	136	104	22.9	16.6	<b>8.9</b>	<b>12.1</b>	<b>23.2</b>	<b>20.4</b>	<b>21.1</b>

### Results of the simulation

The simulation results about the propagation process of the stress wave were shown in Fig. 6 and Fig. 7 when it propagates at the cracks with different depths on the surfaces of specimens  $T_1$  and  $T_2$ . From Fig. 6a, the main propagation modes of stress waves are transverse and longitudinal waves when it propagates on the surface of wood without cracks. The propagation velocity of longitudinal wave is faster (Fang et al. 2023). Li (2021) and others separated longitudinal and transverse waves by the method of PLB tests on different wood surfaces. The results showed that the longitudinal wave velocity of pine wood is about 4.57 times higher than the transverse wave, which is the same as the simulation results in this paper. The main reason for the difference in propagation velocity is the vibration direction of the two acoustic waves. The vibration direction of longitudinal waves is parallel to the wood surface and it is mainly propagated through the axial tracheids within wood. Therefore, the propagation velocity of longitudinal waves is faster in the parallel grain direction and slower in the perpendicular grain direction. This results in an elliptical wavefront curve for stress waves in wood, which is the same as the findings of Liu et al. (2010). The vibration direction of transverse waves in wood is perpendicular to the wood surface and it is damped by mediums such as the axial tracheids and wood rays within wood. As a result, the transverse wave propagation is slower. Additionally, wood is a typical viscoelastic material, and its hindrance to the propagation velocity of transverse waves in the longitudinal direction is more pronounced (O'Ceallaigh et al. 2018). Therefore, with the increase of propagation distance, the longitudinal and transverse waves are significantly separated.

Based on the diffraction wave theory, the diffraction range of the stress wave is different according to different crack depths. Thus, at small crack depths, the propagation mode of the stress wave is in a straight line after bypassing the crack tip, in path  $P_2$ . With increasing crack depth, the diffraction weakens gradually, and the propagation mode of the stress wave is reflection at the right boundary after diffraction at the crack tip, in path  $P_3$ . The propagation paths derived from the simulation results are consistent with the AE experimental. In fact, at the crack, the structure of the orderly arranged tracheids in the wood is destroyed, and

the density are altered (Kami and Toufigh 2022). The energy distribution in different directions changes when the interaction generates between the stress wave and the crack, resulting in diffraction phenomena and changing the propagation path of the stress wave.

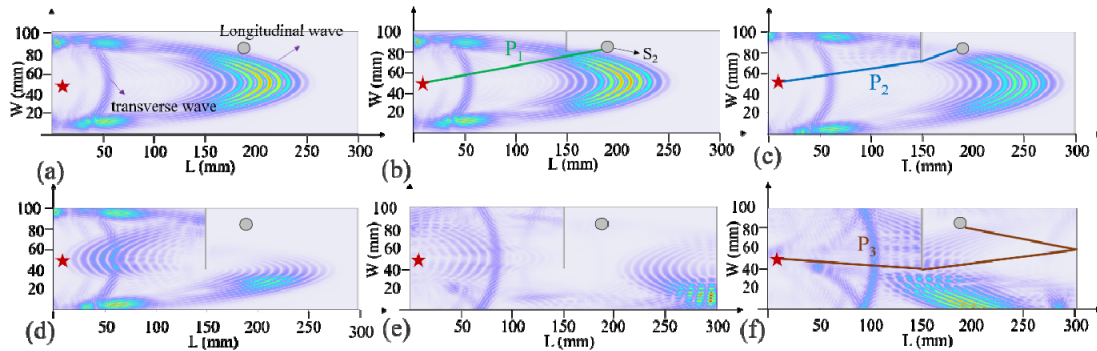


Fig. 6: Simulation for propagation path of stress wave on the surface of specimen  $T_1$ . The crack depth is (a) 0 mm (b) 20 mm (c) 30 mm (d), (e), (f) 60 mm.

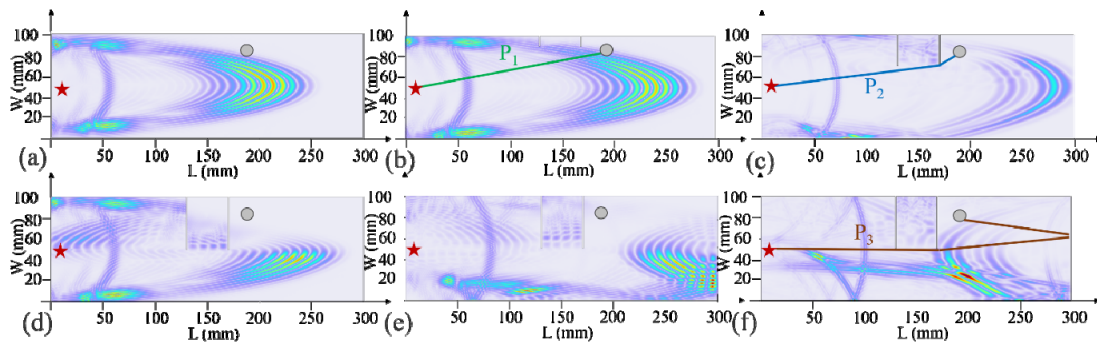


Fig. 7: Simulation for propagation path of stress wave on the surface of specimen  $T_2$ . The crack depth is (a) 0 mm (b) 20 mm (c) 30 mm (d), (e), (f) 50 mm.

The results of Zhao et al. (2022) and others showed that the velocity and energy of the stress waves change significantly by adding boundaries such as aluminum and acoustic cotton on the wood surface. In this paper, cracking is equivalent to the generation of new wood boundaries. The energy distribution of the stress wave near the crack is altered, resulting in a significant change in the propagation path.

### Identifying crack areas wood by time difference

According to the above study, different depths of cracks in wood lead to different propagation paths of stress waves, and the different propagation paths lead to different time differences remarkably. Based on this, the method of identifying the crack depth using AE sensors is proposed in the study, and the experimental schematic is shown in Fig. 8. Specimens  $T_3$  and  $T_4$  were intercepted from pine sawn timber with dimensions of  $400 \times 100 \times 30$  mm, and cracks of arbitrary depth were made in the specimens.

First, two sensors were placed on the specimen surface in order to investigate the estimated position of the crack in the L direction. The distance between the two sensors and the upper boundary of the specimen surface was 10 mm and the spacing was  $l$ . Next, PLB tests were performed at the midpoint between the two sensors and the time of the AE signals

received by the two sensors was calculated. Cracks exist between PLB test points and sensors that arrive later always. Subsequently, the distance between the two sensors was shortened based on the dichotomy method so that the crack was between the sensors always. The PLB test was performed at the midpoint of the two sensors until the distance between the sensors was less than 40 mm. Meanwhile, the estimated position of the crack in the L direction is at the midpoint between the PLB test point and the sensor with late arrival time (Fig. 8c), as well as its maximum error from the actual position is 20 mm (the sensor diameter is 20 mm).

Based on the position of the crack in the L direction, the position of the crack tip in the H direction was explored further, the positions of the sensor and PLB test points relative to the crack are shown in Fig. 8d.

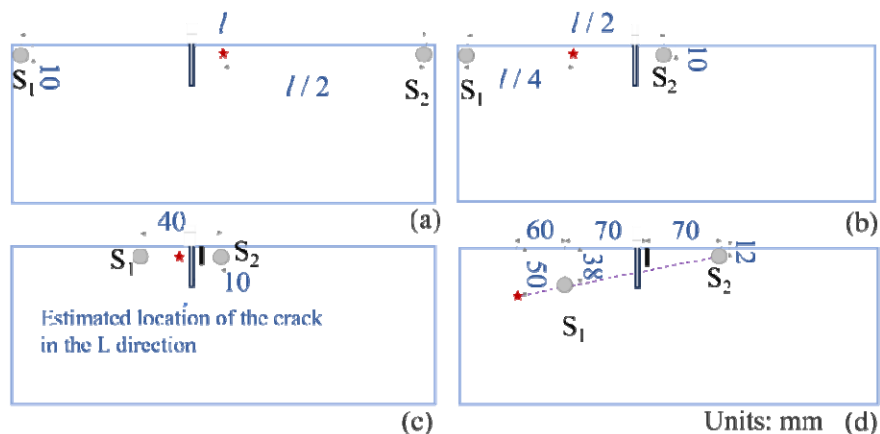


Fig. 8: Experimental scheme of crack depth identification. Units: mm.

Tab.6: Region division for crack depth identification.

Interval number	Time difference range ( $\mu\text{s}$ )	Depth range (mm)
1	32.3	(0, 20]
2	(32.3, 33]	(20, 30]
3	(33, 35.8]	(30, 40]
4	(35.8, 62.8]	(40, 50]
5	(62.8, 68.4]	(50, 60]
6	(68.4, 75.3]	(60, 70]
7	(75.3, 89.5]	(70, 80]
8	(89.5, 94.6]	(80, 90]

The estimated location of the crack tip in the H direction was divided into eight regions, and the time difference range in each region is shown in Tab.6 when the crack depth is less than 90 mm. The actual time difference obtained from the PLB tests method shown in Fig. 8 was used to identify the estimated depth of the crack tip. Depending on the position of the crack tip in the L and H directions, the cracks in the wood can be identified in an area with dimensions of 20×10 mm. As shown in Fig. 9.

Tab.7: Crack identification results

Specimens	Actual time difference ( $\mu\text{s}$ )	Actual depth (mm)	Estimated range of time difference ( $\mu\text{s}$ )	Estimated range of depth (mm)
T <sub>3</sub>	37.5	36	(35.8, 62.8]	(30, 40]
T <sub>4</sub>	63.0	53	(62.8, 68.4]	(50, 60]

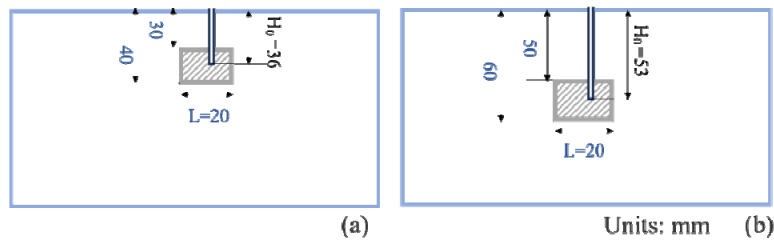


Fig. 9: Crack areas identification results.

## CONCLUSIONS

In order to investigate the effect of crack depth on the stress wave propagation path in wood, the time difference of stress wave propagation at different depths of cracks was investigated in this study by AE experiment. The propagation process of stress waves is explored by COMSOL software based on the method of finite element simulation modeling. The results of the analysis are as follows: (1) In general, stress waves in pine wood are more likely to propagate along the longitudinal direction due to axial tracheids. According to the AE experiment results, the propagation path of the stress wave is affected by the crack depth. Diffraction of the stress wave occurs at the crack tip when the crack depth is smaller. The reflected wave from the end face will reach the sensor faster, while the diffraction of the stress wave is significantly weaker with increasing crack depth. (2) The propagation process of the stress wave is clearly shown according to the results of COMSOL simulation. The propagation velocity of longitudinal waves is faster in wood, and the obstruction effect stems from the fact that the viscoelastic characteristics are stronger for transverse waves. Additionally, cracks at different depths lead to different diffraction ranges of the stress waves, which changes the propagation paths of the stress waves. The propagation paths of cracks at different depths are the same as the conclusions of the AE test. (3) The estimated area of the crack in the L direction was identified based on the dichotomy and TDOA methods; the estimated area of the crack in the H direction was identified based on the time difference of the stress wave in the case of different crack depths. The crack tip was localized in an area of  $20 \times 10$  mm.

Based on this study, the propagation paths of stress waves at different crack depths are explored. Furthermore, a crack depth identification method was proposed. It provides an effective method for monitoring the damage fracture process of wood. In the future research, we are committed to simplifying the experimental process of crack depth identification and improving the accuracy of crack region localization.

## ACKNOWLEDGMENTS

This work was supported by the National Natural Science Foundation of China (32160345, 31760182), Startup fund for introducing talents and scientific research of Anhui University of Engineering (2021YQQ037) and Yunnan Fundamental Research Projects (grant NO. 202401BD070001-121).

## REFERENCES

1. Afoutou, J. S., Dubois, F., Sauvat, N., & Takarli, M. (2023). A novel three-dimensional model for the prediction of ultrasonic velocity in wood considering its orthotropy. *Wood Science and Technology*, 57(3), 605-623.
2. Atreya, N., Wang, P., & Zhu, X. (2023). Characterizing mechanical properties of layered engineered wood using guided waves and genetic algorithm. *Sensors*, 23(22).
3. Dai, J., Liu, J., Zhou, L., & He, X. (2023). Crack pattern recognition based on acoustic emission waveform features. *Rock Mechanics and Rock Engineering*, 56(2), 1063-1076.
4. Fang, S., Li, M., Li, W., Huang, C., Deng, T., & Du, K. (2023). Experimental analysis of acoustic emission propagation velocities and energy attenuation law of P and S waves in wood using improved tdoa measurements. *Wood Research*, 68(1), 112-128.
5. Gao, Y., Fu, Z., Fu, F., Zhou, Y., Gao, X., & Zhou, F. (2022). The formation mechanism of microcracks and fracture morphology of wood during drying. *Drying Technology*, 41(8), 1268-1277.
6. Huang, C., Li, M., Fang, S., Zhao, Y., Qin, G., Yang, Z., Deng, T. (2023). Effects of wood crack size and distribution on the transverse wave characteristics of acoustic emission. *Journal of Northwest Forestry University*, 9, 190-198
7. Han, C., Yang, G., Wang, J., & Guo, X. (2020). The research on propagation characteristics of acoustic emission signals in stiffened plates based on the multipath propagation model. *Ultrasonics*, 108, 106177.
8. Li, H., Li, Q., & Wang Z. (2019). Study on laser ultrasonic testing of metal material surface defects. *Fire Control & Command Contro*. 44(8):61-64.
9. Li, M., Wang, M., Ding, R., Deng, T., Fang, S., Lai, F., & Luo, R. (2021). Study of acoustic emission propagation characteristics and energy attenuation of surface transverse wave and internal longitudinal wave of wood. *Wood Science and Technology*, 55(6), 1619-1637.
10. Liu, Y., & Zhao, G. (2012). *Wood science*. China Forestry Publishing House. China, 398pp.
11. Liu, Z., Pang B., & Tang X. (2010). Acoustic emission source location in laminated plates based on virtual wave front. *Piezoelectrics & Acoustooptics*. 32(3):493-497.
12. O'Ceallaigh, C., Sikora, K., McPolin, D., & Harte, A. M. (2018). An investigation of the viscoelastic creep behaviour of basalt fibre reinforced timber elements. *Construction and Building Materials*, 187, 220-230.
13. Qin, G., Li, M., Fang, S., Deng, T., Huang, C., Mao, F., Xu, N. (2024). Study of a grid-based regional localization method for damage sources during three-point bending tests of wood. *Construction and Building Materials*, 419, 135348.
14. Ramezanzpour Kami, M., & Toufigh, V. (2022). Ultrasonic evaluation for the detection of contact defects of the timber and fiber-reinforced polymer. *Structural Health Monitoring*, 22(4), 2868-2887.
15. Ren, H., Li, T., Ning, J., & Song, S. (2023). Analysis of damage characteristics of steel fiber-reinforced concrete based on acoustic emission. *Engineering Failure Analysis*, 148, 107166.

16. Sahu, S., & Bhattacharyay, R. (2018). Validation of COMSOL code for analyzing liquid metal magnetohydrodynamic flow. *Fusion Engineering and Design*, 127, 151-159.
17. Wang, M., Deng, T., JU, S., Li, X., Li, X., & Li, M. (2020) Effect of wood surface crack on acoustic emission signal propagation characteristics. *Journal of Northeast Forestry University*, 48(10):82-88.
18. Wang, X., Liu, X., He, T., Tai, J., & Shan, Y. (2020). A novel joint localization method for acoustic emission source based on time difference of arrival and beamforming. *Applied Sciences*, 10(22).
19. Wei, X., Sun, L., Sun, Q., Xu, S., Zhou, H., and Du, C. (2019). Propagation velocity model of stress wave in longitudinal section of tree in different angular directions, *BioResources*, 14(4), 8904-8922.
20. Wei, X., Xu, S., Sun, L., Tian, C., & Du, C. (2021) Propagation velocity model and two-dimensional defect imaging of stress wave in larch (*Larix gmelinii*) wood. *Bioresources*, 16(4), 6799-6813.
21. Xu, N., Li, M., Fang, S., Huang, C., Chen, C., Zhao, Y., Wang, Y. (2023). Research on the detection of the hole in wood based on acoustic emission frequency sweeping. *Construction and Building Materials*, 400, 132761.
22. Xu, N., Li, M., Fang, S., Huang, C., Zhao, Y., Mao, F., Wang, Y. (2023). Study the effects of ferrous materials inside wood on the propagation characteristics of acoustic emission signals. *Wood Material Science & Engineering*, 18(5), 1650-1662.
23. Yang, C., Zhu, Z., Liu, J., Xue, B. O., & Li, Y. (2023). Model construction and microwave preheating experiments using fiberboard. *Wood Research*, 68(2), 389-402.
24. Yu, A., Chen, T., Chen, Z., Zhang L., & Chen X. (2023). Study on the effect of cracks on the propagation characteristics of elastic waves in concrete. *Journal of Henan Polytechnic University(Natural Science)*. 1-14
25. Zhang , J., Hao, R., Wu, Z., Green, J., & Li, S. Signal simulation and experimental research on acoustic emission using LS-DYNA. *Journal of Engineering Science and Technology*.
26. Zhang, X. I. N., Li, M., Fang, S., Mao, F., Yang, L., Zhao, Y. U. E., & Qin, G. (2024). Evaluation of wood damage and fracture behavior based on energy entropy of acoustic emission signals. *Wood Research*, 69(2), 283-296.
27. Zhang, Y., Zhao, G.-F., & Li, Q. (2020). Acoustic emission uncovers thermal damage evolution of rock. *International Journal of Rock Mechanics and Mining Sciences*, 132, 104388.
28. Zhao, Y., Li, M., Fang, S., Zhang, S., Huang, C., Deng, T., &Zhu, D. (2022). Influence of boundary conditions on acoustic emission propagation characteristics of *Zelkova schneideriana*. *Journal of Wood Science*, 68(1), 62.

CHUMIN CHEN

<sup>1</sup>SOUTHWEST FORESTRY UNIVERSITY

SCHOOL OF MACHINERY AND TRANSPORTATION

<sup>2</sup>YUNNAN KEY LABORATORY OF WOOD ADHESIVE AND GLUED PRODUCTS  
KUNMING, YUNNAN

MING LI\*

<sup>1</sup>ANHUI POLYTECHNIC UNIVERSITY

SCHOOL OF ELECTRICAL ENGINEERING

<sup>2</sup>KEY LABORATORY OF ADVANCED PERCEPTION AND INTELLIGENT CONTROL  
OF HIGH-END EQUIPMENT OF MINISTRY OF EDUCATION

WUHU, ANHUI

CHINA

\*Corresponding author: swfu\_lm@swfu.edu.cn

SAIYIN FANG\*

<sup>1</sup>YUNNAN KEY LABORATORY OF WOOD ADHESIVE AND GLUED PRODUCTS

<sup>2</sup>SOUTHWEST FORESTRY UNIVERSITY

SCHOOL OF MACHINERY AND TRANSPORTATION

KUNMING, YUNNAN

\*Corresponding author: fsy029@126.com

JIALONG ZHAO, XIN ZHANG, FANGYONG LU, TINGTING DENG

SCHOOL OF MACHINERY AND TRANSPORTATION

SOUTHWEST KUNMING, YUNNAN

CHINA

BO ZHANG

DALIAN UNIVERSITY OF TECHNOLOGY

DALIAN, LIAONING PROVINCE

CHINA